Rotation of defocused wide-field fluorescence images after blinking in single CdSe/ZnS core-shell quantum dots

Xiao-Jun Chen, Yi Xu, Sheng Lan, Qiao-Feng Dai, Xu-Sheng Lin, Qi Guo, and Li-Jun Wu*
Laboratory of Photonic Information Technology, School for Information and Optoelectronic Science and Engineering, South China Normal University, Guangzhou 510006, People's Republic of China
(Received 29 November 2008; published 19 March 2009)

We investigate the emitting dynamics of single CdSe/ZnS core-shell quantum dots (QDs) by employing a defocused wide-field imaging method. A rotation of the defocused images of single QDs after some blinking events is observed, which is direct evidence of the redistribution of carriers in and around single QDs. It is revealed that this change can be considered as a "self-rotation" of the electron cloud (i.e., wave statistic function) around the "dark axis" of the QDs. As all the observed rotations of the emission patterns are accompanied by blinking-off periods, we believe that the rotation of the defocused images and blinking are correlated through redistribution of charged species in and around single QDs.

DOI: 10.1103/PhysRevB.79.115312 PACS number(s): 78.67.Bf, 78.55.−m, 73.21.−b

I. INTRODUCTION

Colloidal semiconductor quantum dots (QDs) have attracted much attention in the last decade due to their unique physical properties and potential applications. A series of photophysics phenomena, such as blinking (fluorescence intermittency),[1] spectral jumping,[2] quantum-confined Stark effect,[3] Stokes shift, etc.,[4] have been observed and interpreted. Among them, blinking is a particularly interesting phenomenon in the fundamental photophysical research and it significantly influences device stability in practical applications. For example, the blinking of QDs may limit their application in nanotechnology and life science.[5] In order to suppress blinking, it is necessary to understand the fluorescence dynamics of QDs, especially singles, and the underlying physical mechanism. The most popular model that describes blinking in semiconductor QDs was developed by Frantsuzov *et al.*,[6] which is called photoionization model. They attributed the photoluminescence (PL) blinking to a random switching between emitting "on" and nonemitting "off" states due to the ionization of QDs under light excitation. Some work has been done to track the optical dynamics of blinking as a function of time in order to investigate the blinking process in detail.[1,7] By measuring the fluorescence intensity and frequency of single QDs simultaneously, a pronounced correlation between fluorescence intermittency and large spectral shifting events has been found.[7] To explain the "cause-and-effect" relationship between these two phenomena, a charge-reorganization model, which is extended from the photoionization model, was proposed. Based on the model, the spectral shift is induced by the redistribution of local electric fields through redistribution of charged species in and around single QDs when they transit from dark to bright states. However, in the process of the transition, the carriers in and around QDs can either be redistributed or be nonredistributed. Furthermore, the process itself and the redistribution of carriers are very hard to observe directly in single QDs. Therefore, it is very difficult to obtain direct evidence of the redistribution of local electric fields. As the redistribution leads to a change in the electron cloud (i.e., wave statistic function), direct observation of the electron cloud of individual QDs will be able to check whether local electric fields are redistributed.

It is well known that much information about electronic energy levels can be retrieved from the PL of QDs.[8,9] Measurements involving a large number of QDs, however, are subject to ensemble averaging, and hence important information about single dots is lost.[10] Since the appearance of the defocused imaging technique based on the wide-field fluorescence microscopy (WFFM), direct observation of the space distribution of the emitting field of single fluorophores has become available. Compared with the conventional orientational imaging with two crossed polarizers, the defocused imaging method allows direct access to the three-dimensional (3D) orientation of the emitters as well as their radiation characteristics within one frame.[11,12] Since this technique is based on the electron transition dipole approximation and the fact that the dipole radiation exhibits an angular anisotropy,[11] the spatial distribution of the emitting field (defocused image) and the deduced polarization characteristic therefore not only provides the information on the geometric structure symmetry of the single QD but also reflects the symmetry of the electron cloud in each QD.[13]

In this paper, we employ the defocused wide-field imaging method (DWFIM) to investigate the dynamics of the emitting field of single CdSe/ZnS core-shell QDs. The defocused image, i.e., emission pattern, of some QDs is observed to rotate after blinking-off periods, implying the redistribution of local electric fields as the defocused image reflects the symmetry of the electron cloud. Since most blinking events are not accompanied by this kind of rotation, it is a low-probability event. This correlation between blinking and rotation of emission patterns suggests that the local electric fields around single QDs can possibly be reorganized when the charged QD transits from a dark to a bright state. Therefore, DWFIM acts as a powerful tool for investigating the distribution of local electric fields around individual QDs.

II. EXPERIMENTAL DETAILS

We fabricated three types of samples in order to exclude the influence of the local environment on QDs, which may

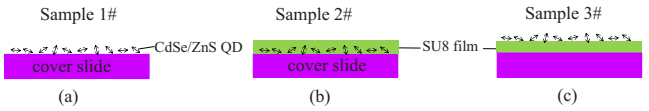

FIG. 1. (Color online) Schematics of three samples. QDs are fixed (a) between the slide (the refractive index $n=1.458$) and air ($n=1.0$), (b) between the slide ($n=1.458$) and the SU8 film ($n=1.6$), and (c) between the SU8 film ($n=1.6$) and air ($n=1.0$), respectively.

modify the photon mode density.[14] Figure 1 depicts their schematic diagrams and the structural parameters are given in the caption. The details of the fabrication procedure are as follows. First, ~ 10 μl of $10^{-9}M$ solution of water-soluble CdSe/ZnS core-shell QDs (WuHan JiaYuan QD Technol. Develop.) was dipped onto a microscope cover slide and then covered by another one. The inside QDs were uniformly distributed on the slides by capillary force. After the solvent was evaporated, two slides were separated and one of them became sample 1. Sample 2 was obtained by spin coating an $\sim$200-nm-thick SU8 (a negative epoxy resin from MicroChem) film on sample 1. For sample 3, the SU8 film was spin coated on the slide first and then followed by the steps fabricating sample 1. Through these procedures, three different environments for QDs were obtained, as shown in Fig. 1.

Defocused wide-field fluorescence images of QDs were measured using a setup depicted in Fig. 2(a). The WFFM is equipped with a Zeiss $100\times/1.4$ NA oil-immersion objective, a long pass filter to block the excitation light in the detection path, an intensified charge-coupled device (CCD) (Carl Zeiss) camera, and a diode-pumped solid-state laser (532 nm, 100 W/cm^2, Coherent). All the fluorescence images were recorded at room temperature. The raw data were collected in a series of consecutive images. The exposure time for each image was set to larger than 100 ms in order to obtain enough signal-to-noise ratio of the PL intensity. The analysis program then retrieves the intensity-time emission trajectories for all the chosen QDs, wherein each data point represents the averaged PL intensity in one selected area. The background intensity was determined locally around each monitored QD. Figure 2(b) shows some typical defocused images of QDs at a focus position of $f\approx -1.2$ μm relative to

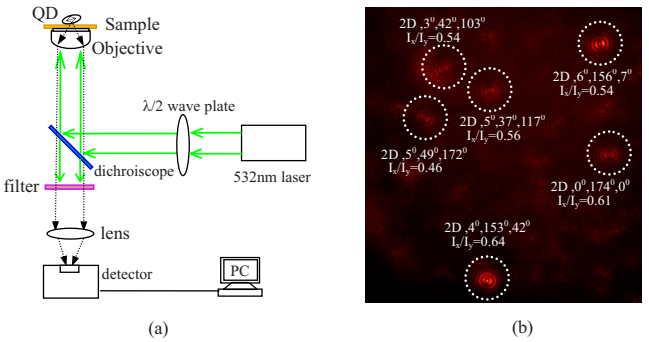

FIG. 2. (Color online) (a) Schematic of the defocused wide-field fluorescence imaging system. (b) Typical defocused images of the CdSe/ZnS QDs obtained in sample 1. The picture was taken with an exposure time of 1.5 s.

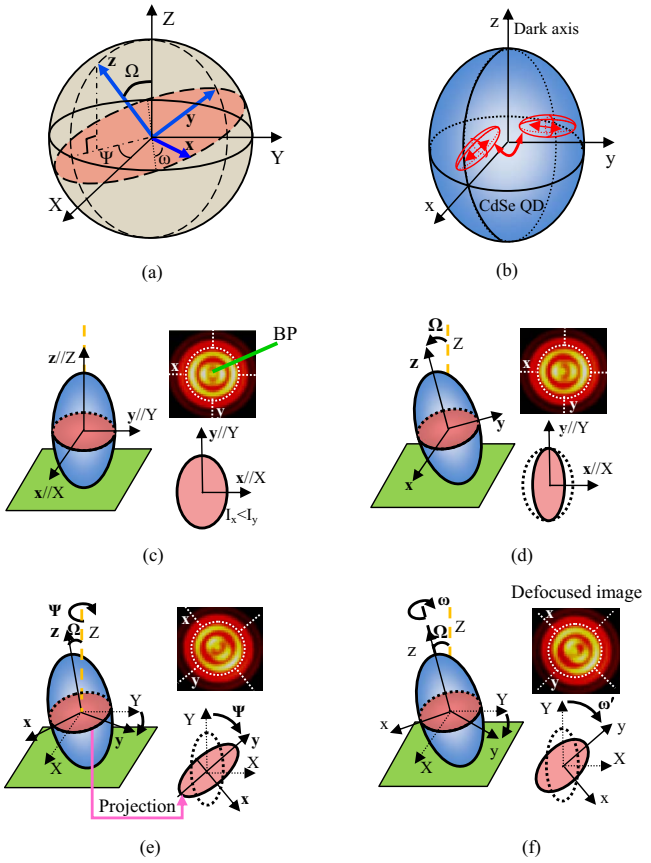

FIG. 3. (Color online) (a) Sketch of the simulation model used to define the emission from a QD. The 3D orientation of the QD's reference system (x,y,z) with respect to the laboratory system (X,Y,Z) is determined by three angles Ω, Ψ, and ω. (b) Sketch of the modified two-dimensional (2D) dipole model in the QD system. The red thick arrow schematically exhibits the correlation between the emissions along x and y axes. [(c)–(f)] The 3D orientations (left) and corresponding calculated defocused images (top right) of different QDs with different Euler angles: (c) $(\Omega,\Psi,\omega)=(0°,0°,0°)$; (d) $(\Omega,\Psi,\omega)=(10°,0°,0°)$; (e) $(\Omega,\Psi,\omega)=(10°,50°,0°)$; and (f) $(\Omega,\Psi,\omega)=(10°,0°,50°)$. Please note that the angle between (X,Y) and (x,y) coordinates is ω', which is the projection of ω onto the observation plane. White dashed circles and lines are guides for eyes.

the focal plane. The minus sign refers to the movement of the sample toward the objective. As can be seen, most of the diffraction patterns show dim-and-bright alternate distribution, which is not only radial but also axial. Obviously, the emitting field of single QDs differs greatly from an ideal spot source.

III. SIMULATION MODEL

The program used to simulate the defocused images is based on the multidimensional dipole model developed by Enderlein and co-workers.[11,15] The orientation of the dipole system with respect to the laboratory system is sketched in Fig. 3(a). As shown, (X,Y,Z) and (x,y,z) indicate the coordinates of the laboratory and dipole systems, respectively. The Z axis is the optical axis. Three Euler angles (Ω,Ψ,ω)

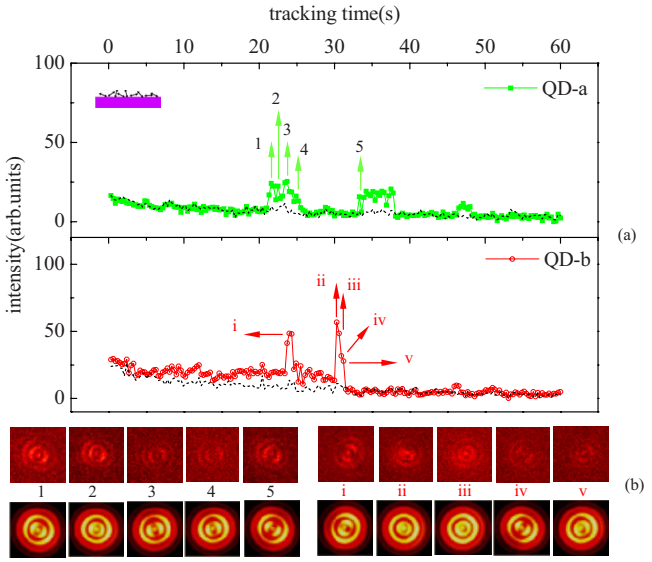

FIG. 4. (Color online) (a) Time traces of the emitting intensities of two representative active QDs (QD-a and QD-b) from sample 1. The black and red solid lines are guides for the eyes. The dashed black lines represent the local background obtained from the immediate surroundings of the monitored QDs. The numbers around the two curves point out the five states shown in (b). Each dot corresponds to one exposure (300 ms). The inset sketches the measured sample. (b) Corresponding evolutions of the defocused emission patterns of the two monitored QDs observed at different times. The images were taken with an exposure time of 300 ms. In each group, top images are the detected states and bottom ones are the corresponding theoretical simulations.

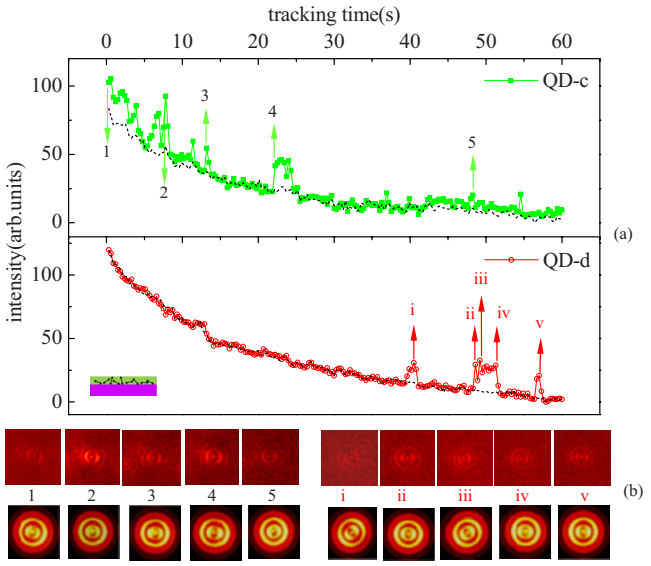

FIG. 5. (Color online) (a) Time traces of the emitting intensities of two active QDs (QD-c and QD-d) from sample 2. (b) The corresponding emission patterns at five selected states.

are defined to establish the relationship between them. As can be seen, the orientation of the z axis with regard to the laboratory system is determined by angles Ω and Ψ. Normally, an ideal 2D model, where a degenerate transition dipole orientates isotropically in two dimensions and thus gives rise to a perpendicular "dark axis" that does not couple to the light field,[16] is sufficient to characterize the emission behavior of a spherical QD ($I_z=0$, $I_x=I_y\neq 0$, where I is the emitting intensity). However, when the 2D transition moment is not of ideal circular shape, the ideal 2D model needs to be modified by introducing an elliptical parameter.[12] Here we apply a modified 2D model with an elliptical parameter to describe the defocused images of QDs ($I_z=0, I_x\neq I_y\neq 0$). It was found that most of the emission patterns in our experiments could be defined by this model precisely. The schematic of a 2D dipole is shown in Fig. 3(b), where the z direction is the dark axis of the structure. The x and y directions are two "bright axes" for either symmetric or asymmetric structure.[15] The elliptical parameter is defined as the ratio of the emitting intensities along the two bright axes (I_x/I_y). Notice that emissions along x and y axes are correlated in the modified 2D model.

The dependence of the defocused images on three Euler angles is schematically demonstrated in Figs. 3(c)–3(f). Bright point "BP" in the defocused images stands for the projection of the dark axis on the observation plane (XOY), as shown in Fig. 3(c). When $\Omega\neq 0$ and $\Psi=\omega=0$, point BP deviates away from the center of the defocused image along x ($\|X$) axis [Fig. 3(d)]. In the case of $\Omega\neq 0$, $\Psi\neq 0$, and $\omega=0$, not only point BP deviates but also bright axes x and y rotate. However, the deviation of point BP is still along the direction of the bright axis x [Fig. 3(e)]. When $\Omega\neq 0$, $\omega\neq 0$, and $\Psi=0$, the deviation of point BP in the defocused image is not along the x axis anymore. At the same time, the brightness of the outer diffractive rings is not symmetric with respect to the bright axes, as shown in Fig. 3(f).

A typical CCD frame with emitting QDs is presented in Fig. 2(b). The simulated results for (Ω,Ψ,ω) and elliptical parameter I_x/I_y according to the experimental parameters are shown beside the diffraction patterns of each QD. It can be seen that most QDs can be described by the modified 2D model.

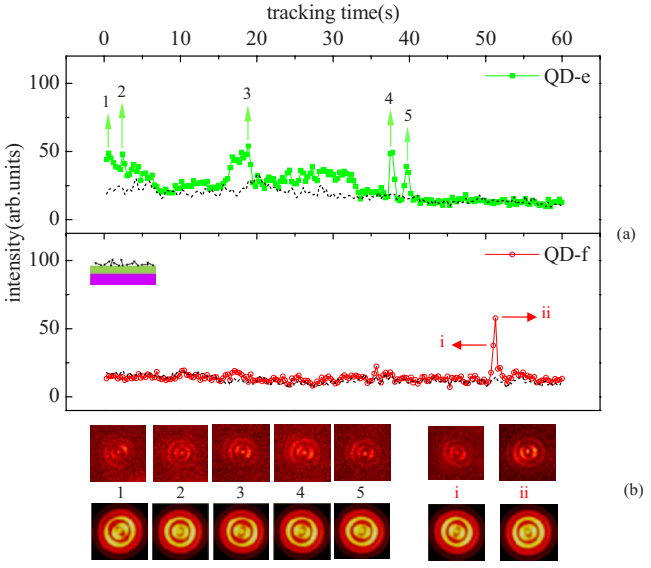

FIG. 6. (Color online) (a) Time traces of the emitting intensities of two representative active QDs (QD-e and QD-f) from sample 3. (b) The corresponding emission patterns at the selected states.

TABLE I. Modeling parameters (Ω,Ψ,ω) and I_x/I_y for each image in sample 1. $\Delta\omega_n=\omega_{n+1}-\omega_n$, where $n=1,2,\ldots$ or i,ii,….

	QD-a: $(\Omega,\Psi)=(4°,32°)$					QD-b: $(\Omega,\Psi)=(7°,20°)$				
n (states)	1	2	3	4	5	i	ii	iii	iv	v
ω (deg)	180	163	130	130	180	79	174	117	16	134
$\Delta\omega_n$ (deg)	17	33	0	−50		85	57	101	−118	
I_x/I_y	0.54	0.67	0.48	0.54	0.43	0.54	0.74	0.82	0.43	0.67

IV. RESULTS AND DISCUSSION

We concentrate our discussion on the active QDs, of which the defocused images changed after blinking-off periods during the observation time, although most of the observed QDs did not show changes in our experiments. The time traces of the PL intensity and corresponding emission patterns of several typical states for six QDs are shown in Figs. 4–6, which summarize the typical phenomenology of emission pattern rotating and blinking in three prepared samples. Each data point in Figs. 4(a), 5(a), and 6(a) represents one exposure (300 ms) and the dashed black lines stand for the local background obtained from the immediate surroundings of each monitored QD. Figures 4(b), 5(b), and 6(b) illustrate the corresponding defocused images of six QDs observed at different times, which are labeled as sequence numbers in Figs. 4(a), 5(a), and 6(a). In each group, the top (bottom) images are the detected (simulated) states. If we inspect carefully the observed images shown in Figs. 4(b), 5(b), and 6(b), no obvious position change (with respect to the outer diffractive ring) for point BP can be found. This is due to the specialty of the dark axis in CdSe QDs. As the temperature of the QD's environment is not close to its glassy transition temperature T_g, the dark axis, which originates from the crystal structure of CdSe QDs, cannot rotate mechanically. Therefore, we can fix angles Ω and Ψ during the simulation as the dark axis is determined by Ω and Ψ (refer to Fig. 3). The simulated results are given in Tables I–III. The change in angle ω between two neighboring states, $\Delta\omega_n=\omega_{n+1}-\omega_n$, is also given in the tables, where $n=1,2,\ldots$ or i,ii,…. The minus (plus) value stands for the anticlockwise (clockwise) rotation. As shown, obvious rotation of the defocused images can be observed in all three samples.

There are several typical types of rotations in the measured QDs. The first type is related with a small rotation angle ($\leq 20°$) of the defocused image after a relatively short dark period. For example, when QD-a evolves from state 1 to state 2, ω rotates by only 17°. At first glance, it seems there is no obvious blinking between these two states. However, the fluctuation of the fluorescence intensity is apparent, implying that some unresolved blinking events have happened during this period. The rotation between states 3 and 4 in QD-c can be considered as the second type, in which ω rotates by a small angle of 5° after a relatively long dark period. In the third type, the defocused images rotate by an angle larger than 20° after a relatively short dark period. For instance, a rotation of −145° between states ii and iii in QD-d belongs to the third type, where the blinking is also not resolved and only the fluctuation of the fluorescence intensity is observed as in the first type. In QD-b, 85° rotation from states i to ii after a relatively long dark period can be considered as the fourth type. It is notable that different types of rotations can occur in the same QD. For example, the first type (from states 1 to 2) and the third type (from states 2 to 3) rotations can both be observed in QD-a. On the other hand, not all blinking events are followed by the rotation of the emission patterns even in some active QDs. As shown in Fig. 6, there are distinct blinking-off periods for QD-e when it evolves from state 3 to state 5. However, no observable rotation is accompanied.

Another remarkable feature we observed in the experiments is that the rotation is also accompanied with variations in the intensity ratio I_x/I_y. As shown in Tables I–III, the value of I_x/I_y is not a constant for each QD, suggesting that the polarization characteristics of the emission change with the rotation of the emission pattern.

When the QDs are embedded in the SU8 film such as in sample 2, the SU8 film can also emit light and form a strong background for the PL intensity of the QDs if it is excited by a high-power laser beam. However, the intensity decreases gradually upon the continuous irradiation, as shown in Fig. 5(a). If the exciting power is not so high, the emitting intensity of the SU8 film is not obvious. As can be seen in Fig. 6(a), the degradation of the PL from the background (SU8 film) is not apparent because the SU8 film was somehow out of focus when we measured the QDs in sample 3.

Overall, the rotation of emission patterns occurs in all three samples, indicating that this phenomenon is insensitive

TABLE II. Modeling parameters (Ω,Ψ,ω) and I_x/I_y for each image in sample 2. $\Delta\omega_n=\omega_{n+1}-\omega_n$.

	QD-c: $(\Omega,\Psi)=(6°,45°)$					QD-d: $(\Omega,\Psi)=(3°,161°)$				
n (states)	1	2	3	4	5	i	ii	iii	iv	v
ω (deg)	152	133	140	145	127	159	23	168	25	20
$\Delta\omega_n$ (deg)	19	−7	5	18		136	−145	143	5	
I_x/I_y	0.6	0.65	0.56	0.54	0.67	0.54	0.63	0.59	0.64	0.57

TABLE III. Modeling parameters (Ω, Ψ, ω) and I_x/I_y for each defocused image in sample 3. $\Delta\omega_n = \omega_{n+1} - \omega_n$.

	QD-e: $(\Omega, \Psi) = (3°, 64°)$					QD-f: $(\Omega, \Psi) = (5°, 25°)$		
n (states)	1	2	3	4	5	i	ii	
ω (deg)	113	164	173	173	173	137	100	Quenched
$\Delta\omega_n$ (deg)	−51	−9	0	0		37		
I_x/I_y	0.6	0.69	0.57	0.6	0.67	0.6	0.67	Quenched

to the environment of QDs. As all the observed rotations of the emission patterns are accompanied by blinking-off periods, we believe that the rotation and blinking of QDs are correlated.

In order to understand the physical mechanism of this correlation, we compare the rotation observed in this work with those reported in other systems such as emitting single-molecule system. In single-molecule experiments, the rotation of defocused images usually occur due to the following reasons: (1) when single molecules are embedded in a polymer near to its glassy transition temperature T_g (rotation diffusion),[17] they can be rotated by the environmental medium mechanically; (2) changing the polarization of the excitation can also induce the rotation of defocused images;[18] and (3) different independent chromophores forming single molecules can radiate orderly because of the energy hopping among them due to the anisotropy of the environment.[19] In our case, however, the experiments were carried out under different conditions. At first, the room temperature is much lower than T_g either for the glass substrate or for the SU8 ($T_g \approx 190$ °C) film. Second, the polarization of the excitation is fixed. Finally, as the emissions of QDs along different axes (I_x and I_y) are correlated, there is no energy hopping between them and the radiation is not ordinal as described in Ref. 19. Therefore, the factors that cause the rotation of defocused images in single molecules are not responsible for the observed rotation in our experiments.

In the photoionization model that describes blinking in semiconductor QDs, a charged QD resulted from Auger ionization is a dark QD. The transition from a dark to a bright QD then occurs through recapture of the initial electron (hole) back into the QD core or through capture of another electron (hole) from nearby traps to neutralize the charged QD core.[20] Based on this model, Neuhauser *et al.* developed the charge-reorganization model to explain the correlation between the large spectral shifting and blinking. There are four possible mechanisms for the charged QDs to transit back to bright. During the transition, a surface dipole can possibly be created and the local electric field can consequently be redistributed.[13] A direct result from the redistribution of the local electric fields is the change in the electron cloud of individual QDs. Indeed, we observed the modification of the electron cloud in single QDs after some blinking events. Since ω is defined as the angle of the x axis with the cross line between the laboratory system and dipole system, its variation can be considered as a "self-rotation" of the electron cloud around the dark axis (z axis). Therefore, the local electric fields around single QDs can really possibly be reorganized when the charged QDs transit back to on states. This is direct evidence not only for the photoionization model that describes blinking in semiconductor QDs but also for its extended charge-reorganization model that describes the correlation between blinking and large spectral shifting.

V. CONCLUSIONS

In summary, we have observed the rotation of the electron cloud by DWFIM. This is a clear manifestation of the redistribution of carriers in and around single QDs. By analyzing the observed defocused images, it was found that the rotation can be ascribed to the change in angle ω, indicating that it can be considered as the self-rotation of the electron cloud around the dark axis. As all the observed rotations of the emission patterns are accompanied by blinking-off periods, we believe that the rotation and blinking of single QDs are correlated and the local electric fields around single QDs can possibly be reorganized when the charged QDs transit from dark to bright states. Therefore, the rotation of the defocused images of QDs observed in our experiments is direct evidence of both the photoionization model and its extended charge-reorganization model, which describes blinking and the correlation between blinking and large spectral shifting, respectively.

ACKNOWLEDGMENTS

The authors acknowledge the financial support from the National Natural Science Foundation of China (Grants No. 10774050 and No. 10674051) and the Program for Innovative Research Team of Higher Education in Guangdong (Grant No. 06CXTD005).

*Corresponding author. ljwu@scnu.edu.cn

[1] M. Nirmal, B. O. Dabbousi, M. G. Bawendi, J. J. Macklin, J. K. Trautman, T. D. Harris, and L. E. Brus, Nature (London) **383**, 802 (1996); Abey Issac, Christian von Borczyskowski, and Frank Cichos, Phys. Rev. B **71**, 161302(R) (2005).

[2] N. Herron, J. C. Calabrese, W. E. Farneth, and Y. Wang, Science **259**, 1426 (2001).

[3] S. A. Empedocles and M. G. Bawendi, Science **278**, 2114 (1997).

[4] Al. L. Efros, M. Rosen, M. Kuno, M. Nirmal, D. J. Norris, and M. Bawendi, Phys. Rev. B **54**, 4843 (1996); E. Johnston-Halperin, D. D. Awschalom, S. A. Crooker, A. L. Efros, M. Rosen, X. Peng, and A. P. Alivisatos, *ibid.* **63**, 205309 (2001).

[5] C. D. Heyes, A. Y. Kobitski, V. V. Breus, and G. U. Nienhaus, Phys. Rev. B **75**, 125431 (2007).

[6] P. Frantsuzov, M. Kuno, B. Jankó, and R. A. Marcus, Nat. Phys. **4**, 519 (2008).

[7] R. G. Neuhauser, K. T. Shimizu, W. K. Woo, S. A. Empedocles, and M. G. Bawendi, Phys. Rev. Lett. **85**, 3301 (2000).

[8] Al. L. Efros and A. V. Rodina, Phys. Rev. B **47**, 10005 (1993).

[9] V. Zwiller, L. Jarlskog, M.-E. Pistol, C. Pryor, P. Castrillo, W. Seifert, and L. Samuelson, Phys. Rev. B **63**, 233301 (2001).

[10] S. A. Empedocles, D. J. Norris, and M. G. Bawendi, Phys. Rev. Lett. **77**, 3873 (1996); O. Labeau, P. Tamarat, and B. Lounis, *ibid.* **90**, 257404 (2003).

[11] D. Patra, I. Gregor, J. Enderlein, and M. Sauer, Appl. Phys. Lett. **87**, 101103 (2005).

[12] R. Schuster, M. Barth, A. Gruber, and F. Cichos, Chem. Phys. Lett. **413**, 280 (2005).

[13] J. T. Hu, L. S. Li, W. D. Yang, L. Manna, L. W. Wang, and A. P. Alivisatos, Science **292**, 2060 (2001).

[14] W. L. Barnes, J. Mod. Opt. **45**, 661 (1998).

[15] M. Böhmer and J. Enderlein, J. Opt. Soc. Am. B **20**, 554 (2003).

[16] J. Tittel, W. Gohde, F. Koberling, A. Mews, A. Kornowski, H. Weller, A. Eychmuller, and Th. Basche, Ber. Bunsenges. Phys. Chem **101**, 1626 (1997).

[17] A. P. Bartko, K. Xu, and R. M. Dickson, Phys. Rev. Lett. **89**, 026101 (2002).

[18] R. J. Pfab, C. Hettich, I. Gerhardt, A. Renn, and V. Sandoghdar, Chem. Phys. Lett. **387**, 490 (2004).

[19] W. Schroeyers, R. Vallee, D. Patra, J. Hofkens, S. Habuchi, T. Vosch, M. Cotlet, K. Müllen, J. Enderlein, and F. C. De Schryver, J. Am. Chem. Soc. **126**, 14310 (2004).

[20] Al. L. Efros and M. Rosen, Phys. Rev. Lett. **78**, 1110 (1997).